Bulletin of Volcanology (2022) 84:84
https://doi.org/10.1007/s00445-022-01592-2

RESEARCH ARTICLE

Links between volcanic activity and flank creep behavior at Pacaya Volcano, Guatemala

Judit Gonzalez-Santana[1] · **Christelle Wauthier**[1,2] · **Michelle Burns**[1]

Received: 2 December 2021 / Accepted: 20 July 2022

Abstract

Magmatism is a recognized potential driver of volcanic flank instability. Recently, this driver was identified at Pacaya Volcano, Guatemala, where a large eruption in 2014 accelerated southwest flank creep. This work investigates the links between flank creep and eruptive behavior at Pacaya to better understand the conditions under which flank creep can be initiated, sustained, or halted at active volcanoes. Time-series of surface displacements from 2007 to 2020 computed using seven Synthetic Aperture Radar datasets are compared with volcanic activity reports, ash advisories, thermal anomalies, and lava flow maps. We find that large transient flank instabilities occurred during vigorous eruptions in 2010 and 2014, but not during times of similarly elevated activity in 2007–2009 and 2018–2020. Flank creep continued years after the two transient instability events, during the relatively quiescent intervals of 2010–2014 and 2015–2018. During periods of elevated volcanic unrest attributed to open-vent volcanic activity, as in 2007–2009 and 2018–2020, magma migrates in an open conduit with little associated deformation or flank motion. Conversely, the opening of new vents outside the summit area, irrespective of whether this marks the start or a transition in an eruption, can initiate transient flank creep as in 2010 and 2014. Thus, future opening of new magma pathways, particularly in a north-northwest to south-southeast alignment, might provide forewarning for an increased likelihood of renewed or accelerating flank creep at Pacaya.

Keywords InSAR · Time-series analysis · Remote sensing · Volcano geodesy · Flank instability · Lava flow mapping

Introduction

Long-term monitoring of volcanic flanks with evidence of past failure is essential. Over 20,000 lives have been claimed by large debris avalanches (> 0.1 km^3) resulting from volcanic edifice failure in the past 400 years (Siebert et al. 1987). Repeated volcanic flank collapses have also been reported at oceanic island and inland volcanoes such as Mount Taranaki, Colima, and Stromboli (Zernack & Procter 2021).

Of the 28 collapse events identified since 1500 AD (Siebert et al. 1987), 75% coincided with volcanic eruptions, highlighting the prevalence of magmatism as a driver for catastrophic flank collapse (Dufresne et al. 2020). Field, lab, and numerical studies have related instability to both the intrusion and extrusion of magma, which can directly cause overloading, over-steepening and deformation, as well as mechanically or thermally alter the edifice (e.g., Elsworth & Voight 1995; McGuire 2003; Roverato et al. 2020). Flank instability can also present itself as slow on-going creep or transient slip events, often due to repeated dike intrusions along volcanic rift zones (McGuire 2003; Poland et al. 2017). Magmatism is a recognized driver of this style of instability at volcanoes such as Kilauea (Hawaii), Piton de la Fournaise (Réunion), and Etna (Sicily) (Poland et al. 2017), and has most recently been proposed for Pacaya (Guatemala) (Gonzalez-Santana & Wauthier 2021).

Radar satellite geodesy first revealed transient flank instability events at Pacaya during vigorous explosive eruptions in May 2010 and January–March 2014 (Schaefer et al. 2015; Wnuk & Wauthier 2017). Smaller magnitude flank creep

---

This paper constitutes part of a topical collection:

Volcanic processes: tectonics, deformation, geodesy, unrest

Editorial responsibility: J. Ruch

✉ Judit Gonzalez-Santana
jmg6885@psu.edu

[1] Department of Geosciences, The Pennsylvania State University, State College, PA, USA

[2] Institute for Computational and Data Sciences, The Pennsylvania State University, State College, PA, USA

between 2011 and 2014 was later identified, with increased slip rate during an intense eruptive phase in 2014 suggesting that magma intrusions promote flank slip (Gonzalez-Santana & Wauthier 2021). Given the evidence for past collapse of the southwest flank of the ancestral Pacaya Volcano, it is essential to evaluate the response of present-day flank creep to changes in volcanic behavior, to better understand the conditions under which another collapse might happen.

To capture the evolution of flank instability at Pacaya, we process radar satellite datasets spanning over a decade from 2007 to 2020, an extension to the 2011–2014 time series presented in Gonzalez-Santana and Wauthier (2021). The observed displacements are compared with volcanic activity reports, ash advisories, thermal anomalies, and lava flow maps to identify the processes contributing to flank creep behavior changes at Pacaya. In particular: (1) whether flank creep initiated during the 2010 eruption, (2) whether it has been on-going beyond the 2014 eruptions, and (3) how the initiation, persistence, and stalling of flank creep relate to changes in eruptive behavior.

Geological background and eruptive history of Pacaya

Pacaya is part of the Central American Volcanic Arc and is one of the most active volcanoes in Guatemala, located only 30 km south of the capital city on the southern rim of the Amatitlán caldera (Siebert et al. 2006; Vallance et al. 1995). The Pacaya volcanic complex is Holocene in age and made up of an ancestral andesitic stratovolcano, rhyodacitic-andesitic domes, and the modern Pacaya volcano (2552 m) (Fig. 1) (Conway et al. 1992; Eggers 1971). Pacaya's scarp formed during the catastrophic collapse of the southwest flank of the ancestral Pacaya volcano between 0.6 and 1.6 ka, which led to a > 0.65 km^3 debris avalanche that traveled > 25 km from the active cone and was accompanied by phreatic-phreatomagmatic explosions and lateral surges (Kitamura & Matias 1995; Rose et al. 2013; Siebert et al. 2006; Vallance et al. 1995). Following this collapse, a return to the volcano's typical Strombolian activity built the modern Pacaya cone, the Mackenney cone, within the scarp (Kitamura & Matias 1995; Siebert et al. 2006; Vallance et al. 1995).

Volcanic unrest at Pacaya is episodic, with eruptive periods lasting 50–300 years, and dormant periods lasting 300–500 years (Conway et al. 1992; Vallance et al. 1995). Pacaya has been persistently active since 1965 (Bardintzeff & Deniel 1992; Rose et al. 2013) with frequent lava flows, Strombolian explosions, and ash plumes (Global Volcanism Program 2013). Most eruptive vents are within hundreds of meters of the Mackenney cone, with less than 5% of vents opening < 2200 m above sea level, but it is these vents that produced many of the largest flows (> 10^5 m^3) (Matías Gomez et al. 2012).

Volcanic activity from 2007 to 2020

Volcanic activity reports from 2007 to 2020 were compiled from INSIVUMEH bulletins (https://insivumeh.gob.gt/)

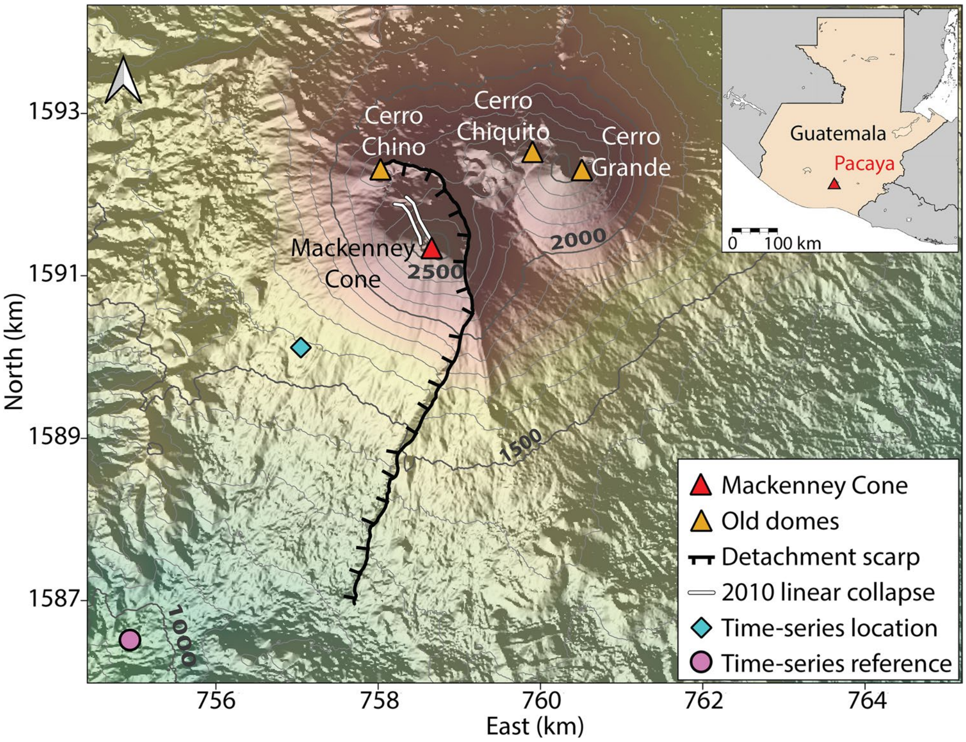

Fig. 1 Map of the Pacaya Complex and its location within Guatemala. The blue diamond shows the area for which InSAR time-series are plotted (Figs. 4 and 5) and the pink circle shows the reference location

and Global Volcanism Program (GVP) weekly reports and special bulletins (Global Volcanism Program 2013). INSIVUMEH, the Guatemalan agency in charge of volcano monitoring, produces daily, weekly, monthly, and special bulletins, published in Spanish. GVP compiles weekly reports and bulletin reports, based on INSIVUMEH data; however, GVP does not receive and record all the data collected by observatories (Reath et al. 2019a, b) and these data must also be translated to English, which might lead to errors. Many of these reports are also based on visual observations and thus may be incomplete on days with inclement weather. Mentions of observed explosions, ash venting, lava flows, incandescence, fumarolic or degassing activity, and tremor were recorded (Fig. 2). These compilations are also provided as Supplementary Materials 2 and 3.

Activity from 2007 to 2009 consisted of intermittent Strombolian explosions with lava flows originating from the Mackenney cone and confined within the collapse scarp (Global Volcanism Program 2013). On April 2010, abundant lava effusion and increased seismicity provided warning for the upcoming eruptions of May 27 and 28. These VEI 2–3 eruptions produced the largest amounts of lava effusion since 1961, from vents outside of the collapse scarp, and generated a 3-km-high ash plume (Matías Gomez et al. 2012; Wardman et al. 2012). The explosions were accompanied by collapse of the west side of the Mackenney crater, producing a north-northwest trending trough (Fig. 1) (Schaefer et al. 2015; Wardman et al. 2012). Explosions were intermittent through the end of the eruptive period on October 2010 (Global Volcanism Program 2013).

In 2011–2013, unrest only consisted of intermittent seismicity pulses, fumarolic plumes, and gas emissions. Gas and ash plumes on March 2013 led to intermittent lava flow effusion, incandescence, and explosions that culminated in more vigorous mixed effusive-explosive activity between January and March 2014, destroying the cone inside the Mackenney crater (Global Volcanism Program 2013). On January 4, 2014, 4-km-long lava flows were produced, and ash and gas plumes rose 3.4 km (Global Volcanism Program 2013; Wnuk & Wauthier 2017). Increased gas and vapor plumes and ejection of pyroclastic material took place in late February, followed by Strombolian explosions on March 2, with ash rising > 2.5 km and lava effusion on the west flank (Global Volcanism Program 2013; Wnuk & Wauthier 2017). Intermittent ash plumes were observed through February 2015 (Global Volcanism Program 2013).

The latest eruptive period began with renewed incandescence and intermittent ash venting in June 2015.

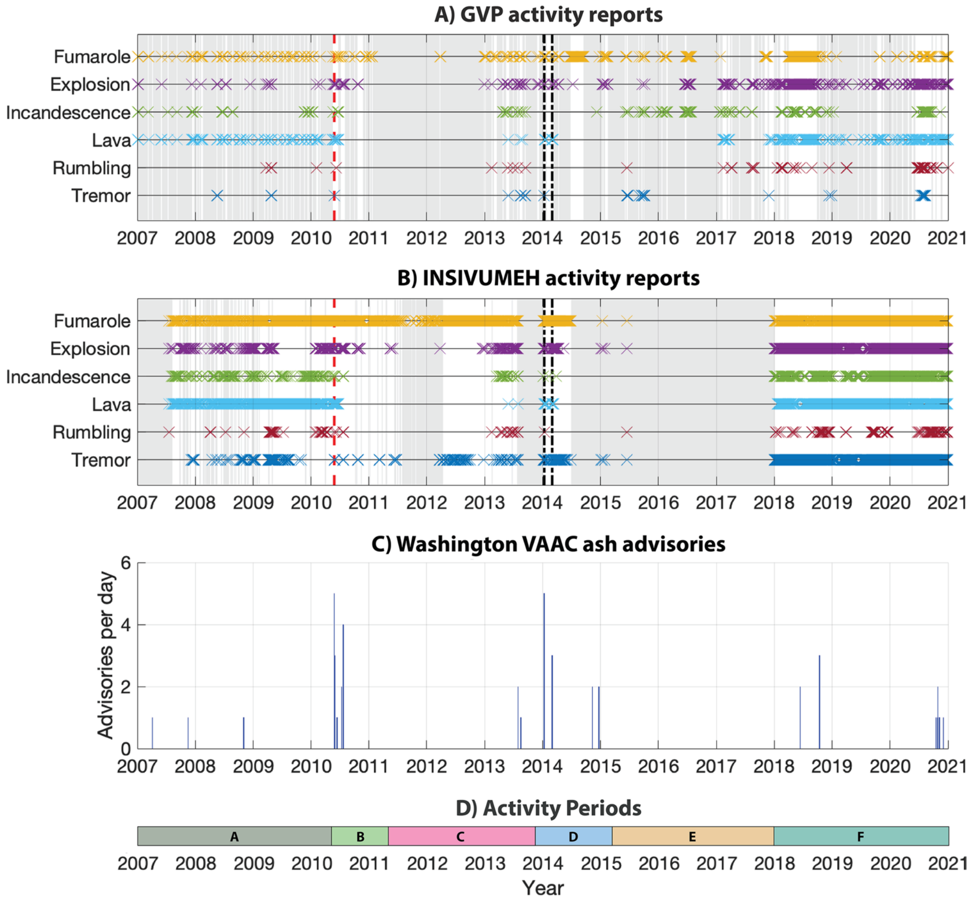

Fig. 2 Volcanic activity at Pacaya reported by the following: **A** the Smithsonian GVP and **B** INSIVUMEH. Grey bars mark intervals of > 2 consecutive days with no available reports. Vertical dashed lines highlight the timing of large eruptions in May 2010 (red) and January and March 2014 (black). Additional details are given in the Supplementary Materials. **C** The number of daily ash advisories for Pacaya generated by the Washington VAAC. **D** Main activity periods referred to in the text, corresponding to transitions in flank displacement rates

Incandescence became more prevalent toward the end of 2015, and a growing intra-crater cone produced Strombolian activity throughout 2016, filling most of the crater by 2017. Explosions persisted throughout 2017 and new lava flows erupted around the summit in January-April 2017, with effusion of flows < 1 km from November 2017, and persistent Strombolian activity from 2019 to 2020 (Global Volcanism Program 2013). Lava effusion and increased explosive activity were observed during August–November 2020, with a substantial increase in vigor (flows > 1 km long) in December 2020 (Global Volcanism Program 2013).

Remote-sensing data and methods

InSAR time-series analysis

To capture the evolution of small magnitude displacements over a decadal period, we performed Interferometric Synthetic Aperture Radar (InSAR) time-series analysis using the Small BAselines Subset (SBAS) method (Berardino et al. 2002; Lundgren et al. 2001). This technique relies on selecting image pairs with small perpendicular (perpendicular distance between the satellite positions) and temporal (time between acquisitions) baselines in order to minimize geometric and temporal decorrelation, respectively (Berardino et al. 2002), which is critical in tropical regions of Central America (Ebmeier et al. 2013a). SBAS requires SAR data from satellite platforms with recurrent repeat passes in the same orbit, such that a well-connected network of interferograms (each scene can be interfered with at least two other scenes) can be produced, which for Pacaya happens after 2007 (see Table 1 and Fig. 3).

SAR pairs were processed using GAMMA (Werner et al. 2001). Topographic contributions were removed using a 12 m TanDEM-X digital elevation model and interferograms were smoothed with an adaptive spectral filter strength 0.4 (Goldstein & Werner 1998). Unwrapping of the InSAR phase was performed with a Minimum Cost Flow algorithm (Costantini 1998) on a triangular irregular network (Costantini & Rosen 1999). The line-of-sight (LOS) displacement field in radians was converted to centimeters and the coherence threshold set to 0.3.

SBAS time-series analysis was performed individually on each dataset, yielding LOS displacements over time for each pixel that remained coherent in all the interferograms in that dataset. LOS displacements between acquisitions were obtained through a pixel-by-pixel linear least-squares inversion of the mean phase velocity for each time interval between dates, through singular value decomposition, with the first date chosen as reference (Berardino et al. 2002).

For cases where at least one ascending and descending dataset overlap in time, an extension to the SBAS method,

Table 1 SAR datasets used in this study. The daisy-chain method links each acquisition to the 3 prior and 3 later dates. $B_\perp$ = perpendicular baseline, T = temporal baseline

Satellite	Start date	End date	Dates	Interferograms	$B_\perp$	T	Heading (°)	Incidence (°)	Orbit/Frame (Swath)	Wave-length (cm)	Polarization	Acquisition mode
ALOS-1	2007–02-03	2011–04-01	19	40	700	300	−11.0	38.8	172/270	23.6	HH	Fine Beam
d-RSAT2	2010–09-26	2015–06-20	32	187	200	300	−168.7	38.4	N1439W09061	5.6	HH	Fine Beam (F1)
d-CSK	2011–06-08	2015–09-30	99	365	300	200	−168.8	26.7	N/A	3.1	HH	Stripmap (HIMAGE)
a-CSK	2014–01-21	2015–10-11	76	281	180	180	−11.3	24.0	N/A	3.1	HH	Stripmap (HIMAGE)
a-RSAT2	2014–06-13	2017–11-12	50	228	150	180	−11.5	37.6	N1435W09061	5.6	HH	Fine Beam (F1)
a-S1	2015–04-25	2020–12-30	218	648	Daisy-chain		−12.1	39.3	136 (IW2)	5.6	VV	ScanSAR
d-S1	2014–10-31	2020–12-28	215	639	Daisy-chain		−167.9	39.3	26 (IW2)	5.6	VV	ScanSAR

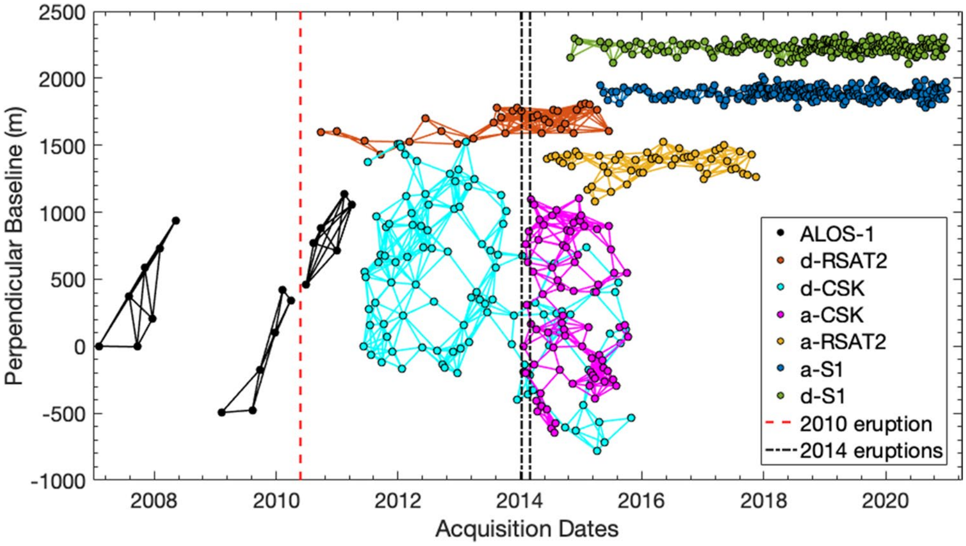

Fig. 3 Baselines of all SAR datasets in this study. Each circle represents an acquisition. Lines join pairs of acquisitions below the perpendicular and temporal baseline thresholds set for each dataset (Table 1), representing interferograms. The dashed vertical lines show the timing of the May 2010 (red) and January–March 2014 (black) eruptions. The ALOS dataset is split into 3 separate non-overlapping networks. Subsequent datasets were vertically offset from their 0 starting perpendicular baseline for clarity

the Multidimensional SBAS (MSBAS, software version MSBASv3 (Samsonov 2019)), allows retrieval of the horizontal and vertical velocity components (Samsonov & d'Oreye 2012, 2017). Note that MSBAS neglects the north–south component of motion since SAR platforms are on near-polar orbits. MSBAS was applied on the ascending and descending RSAT2, CSK, and Sentinel-1 (S1) datasets, overlapping from 2014 to 2020. For all datasets, the same reference region at the foot of the southwest flank of the volcano was used (Fig. 1).

Ash advisories

To overcome some of the bias from relying on visual observations, and availability of written reports, we compiled the number of daily volcanic ash advisories from the Washington Volcanic Ash Advisory Center (VAAC) (NOAA 2021). This allows a more robust identification of dates with explosive ash-producing eruptions at Pacaya. VAACs monitor the presence of volcanic ash in their airspace to communicate volcanic hazards to the aviation community. Ash detection is based on GOES satellite data, which have high enough resolution to distinguish ash plumes from Pacaya and neighboring Fuego volcano when they are both active (Peter Argueta, personal communication, March 2022). However, detection is limited to events that produce plumes detectable from space and overlapping with image acquisition times. Thus, smaller, dilute ash plumes on days with thick cloud cover can be missed. However, advisories sometimes include reports from visual or web-cam observations.

Thermal time-series

To investigate the evolution of thermal anomalies at Pacaya, we combined two thermal remote sensing datasets using NASA thermal infrared (TIR) and middle infrared (MIR) instruments to maximize the completeness of our thermal anomaly catalogue: (1) the Advanced Spaceborne Thermal Emission and Reflection Radiometer (ASTER) on board the Terra satellite, and (2) the Moderate Resolution Imaging Spectroradiometer (MODIS) on board Terra and Aqua satellites. ASTER has a 90-m TIR spatial resolution and a temporal resolution of ~ 16 days at Pacaya, whereas MODIS data have 1-km TIR spatial resolution and bi-daily temporal resolution (Coppola et al. 2012; Reath et al. 2019a, b). The most sensitive automated hotspot detection algorithm that uses MODIS data, MIROVA, detects anomalies > 20°C above the background surface temperature, whereas ASTER has a sensitivity of ~ 2°C (Reath et al. 2019a, b). Therefore, ASTER provides greater sensitivity to changes in thermal activity but sparser time-series (Reath et al. 2019a, b).

MODIS thermal data were obtained from two automatic volcanic-hotspot detection systems: MODVOLC (Wright 2016; Wright et al. 2004) and MIROVA (Coppola et al. 2012, 2016). We inspected the MIROVA Volcanic Radiative Power (VRP) and produced rank ordered statistical plots to reveal subdivisions in the data that might reflect different eruptive regimes (Coppola et al. 2012). Events of the same type are expected to follow a linear trend, with distinct trends (changes in slope) suggesting changes in the nature of the volcanic activity (Coppola et al. 2012). To gauge the temporal persistence of the thermal anomalies, we calculated the monthly frequency of MODIS observations that resulted in alerts (Alert Frequency, i.e., the percentage of nights each month with a night-time MIROVA alert). During lava flow effusion periods lasting over a month, the alerted frequency should be 100%; however, heavy cloud or volcanic plume cover will affect the detection ability, thus this parameter can provide insights into the proportion of scenes that are masked by clouds (Coppola et al.

2012), which can vary seasonally. Finally, we integrated the monthly VRP from 2007 to 2020 to identify periods with largest contributions to the Cumulative Radiated Energy (CRE) (Coppola et al. 2012). For MODVOLC, we recorded hotspot alerts.

Following Reath et al. (2019a, b), we manually calculated temperature above background values at Pacaya using ASTER TIR data (Gillespie et al. 1998). We inspected night-time, cloud-free, kinetic surface temperature (AST_08) products and subtracted the average temperature of a 10 × 10 pixel area near the observed thermal anomaly from the maximum value in the anomaly. We focused on thermal anomalies near the summit crater to ensure the anomalies reflect enhanced volcanism in the vicinity of the main eruptive vents instead of days-old lava flows.

Lava flow and vent maps

Lava flow and vent shapefiles for Pacaya were available for flows between 1961 and 2010 (Matías Gomez et al., 2012) and for the January–March 2014 eruptions (Wnuk & Wauthier 2017). Vent locations through January 2019 were provided by Carla Chun (Chun 2020). We produced shapefiles for the remainder of lava flows and vents from 2006 to 2020, using imagery from Sentinel-2, Landsat-8, and ASTER. False color band combinations were made from Sentinel-2 and Landsat-8 imagery to highlight the location of thermal anomalies and ASTER Kinetic Surface Temperature data was used directly. Lava flow shapefiles were created by tracing around each identified lava flow in ArcMap and the topographically highest point on each lava flow was used as its eruptive vent location. See the Supplementary Material for more details and access to the shapefile repository.

Results

InSAR time-series analysis

Figure 4 shows the LOS SBAS time-series displacements for all SAR datasets, for a 10 × 10 pixel time-series location on the southwest flank of Pacaya (Fig. 1), overlaid manually on the same plot. Negative LOS displacements correspond to a range increase (ground moving away from the satellite). The ALOS dataset was processed as three separate networks to preserve coherence closer to the summit, which was lost during the 2010 eruption. Offsets between the three ALOS subsets are unknown and were arbitrarily set to zero. The sparseness of these subsets impedes drawing firm conclusions, but overall, we observe little displacement from 2007 to mid-2008 and range decrease of ~ 4 cm from 2009 to mid-2010 (period A) (Fig. 4). The southwest flank experienced ~ 12 cm/year range increase from mid-2010 to early 2011 (period B), decaying to ~ 1.8 cm/year until December 2013 (period C). Range increase rates increased to ~ 6.0 cm/year around the 2014 eruption and sustained through 2015 (period D). From 2015 to 2018, range increase continued at ~ 1.2 cm/year (period E), before flattening to ~ 0.2 cm/year (period F). Figure 5 shows the joint MSBAS time-series vertical and horizontal displacements for the overlapping CSK, RSAT2 (descending only), and S1 datasets. The ascending RSAT2 dataset (Fig. S12) was omitted from joint processing given its lower signal to noise ratio. Superimposed on the displacement trends described above, we observe annual cyclicity signals of ~ 2.5-cm amplitude, that are most visible once observations become denser after 2015 (Fig. 4) and in the vertical (Fig. 5). Individual SBAS time-series plots, cumulative displacement maps, additional MSBAS plots, and alternative time-series plots for 6 other locations

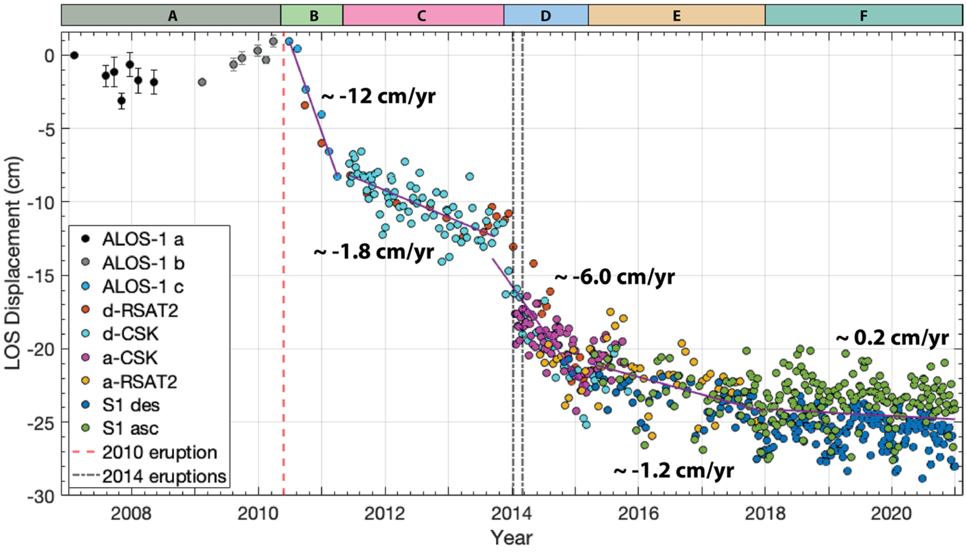

Fig. 4 SBAS time-series plot of LOS displacements for all datasets for the time-series area in Fig. 1, overlain with purple linear regression lines used to calculate the approximate LOS displacement rates for 5 identified linear displacement periods (**B**–**F**). Individual datasets were manually offset from their default initial zero displacement by visual correlation. The offset between ALOS subsets was set to 0

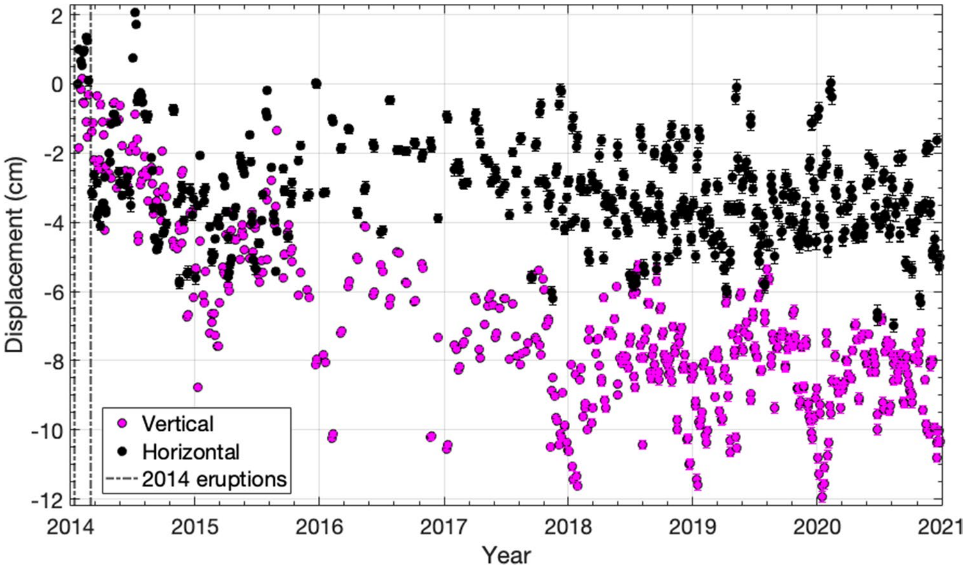

Fig. 5 MSBAS time-series plot of vertical and horizontal (east–west) displacements for the time-series area in Fig. 1 from descending RADARSAT-2, both COSMO-SkyMed, and both Sentinel-1 datasets

on Pacaya are included in the Supplementary Material (Figs. S4-S22). In all time-series plots, the error bars represent the standard deviation in displacements amongst the 10 × 10 time-series pixels.

Volcanic activity and ash advisories

We observe three periods of heightened eruptive activity: 2007–2010 (A and B), around the 2014 eruption (D), and 2018–2020 (F), following a small burst of activity in early 2017 (Fig. 2). Low activity periods (C and E) typically present degassing in the form of fumarolic plumes and occasional ash venting. High activity periods are characterized by explosive activity, such as Strombolian eruptions, sometimes accompanied by ash, and lava flow effusion. Incandescence is often observed at the summit crater, during Strombolian bursts, and reflecting off lava flows at night. Rumbling and other noises often accompany periods with Strombolian explosions, whereas tremor is ascribed to sources such as degassing, magma ascent, explosions, and drag from lava flow movement. The number of VAAC ash advisories from 2007 to 2020 further highlight the eruptive vigor during periods B, D, and F, with most advisories happening during the 2010 and 2014 eruptions (Fig. 2C).

Thermal anomalies

MIROVA data (Fig. 6) allow us to investigate the evolution of thermal anomalies and identify different thermal regimes at Pacaya. Comparisons between MIROVA VRP, MODVOLC alert timing, and ASTER temperature above background are included in the Supplementary Material. All datasets show three periods of heightened thermal output: 2007–2010 (period A into the start of B), around the 2014 eruption (start of D) and 2018–2020 (F) (Fig. S2).

Statistical analysis of MIROVA data reveals four thermal anomaly regimes (Figs. 6A, B). Alerts < 1 MW are related to satellite acquisitions during cloudy conditions or under extreme viewing geometries which hamper detection of clear anomalies (Coppola et al., 2012; Naismith et al. 2019) (Fig. 6A). Alerts between 1 and 25 MW occur pervasively throughout periods of detected alerts, including the start and end of higher VRP intervals, such as the January–March 2014 eruptions, around the start of 2016, and 2017. Alerts with 25–350 MW are frequent from 2007 through the May 2010 eruption, and from 2018 onwards, with occurrences before the 2014 eruption, at the start of 2015 and 2017. Alerts with > 350 MW are only reported in early 2014 and mid-2018. The largest monthly averaged VRP values are recorded just before 2010 and at the start of 2014 (Fig. 6C). Monthly averages are also relatively elevated from 2007 through May 2010, at the start of 2015, and from 2018 onwards. The CRE shows that the greatest contribution to the total energy output is from the near-constant VRP alerts leading to the 2010 eruption, with emissions since 2018 showing a less steep gradient, and with the 2014 eruption contributing to the total output in the form of a clear step. Despite written reports of persistent lava flow activity during heightened activity periods at Pacaya (e.g., A: 2006–2010, F: 2018–2020), no months show alert frequencies greater than 70% (Fig. 6D). Alert frequencies above 50% are noted in the boreal winter months from 2007 to 2010, and from 2018 to 2020, with frequencies dropping in the boreal summer months.

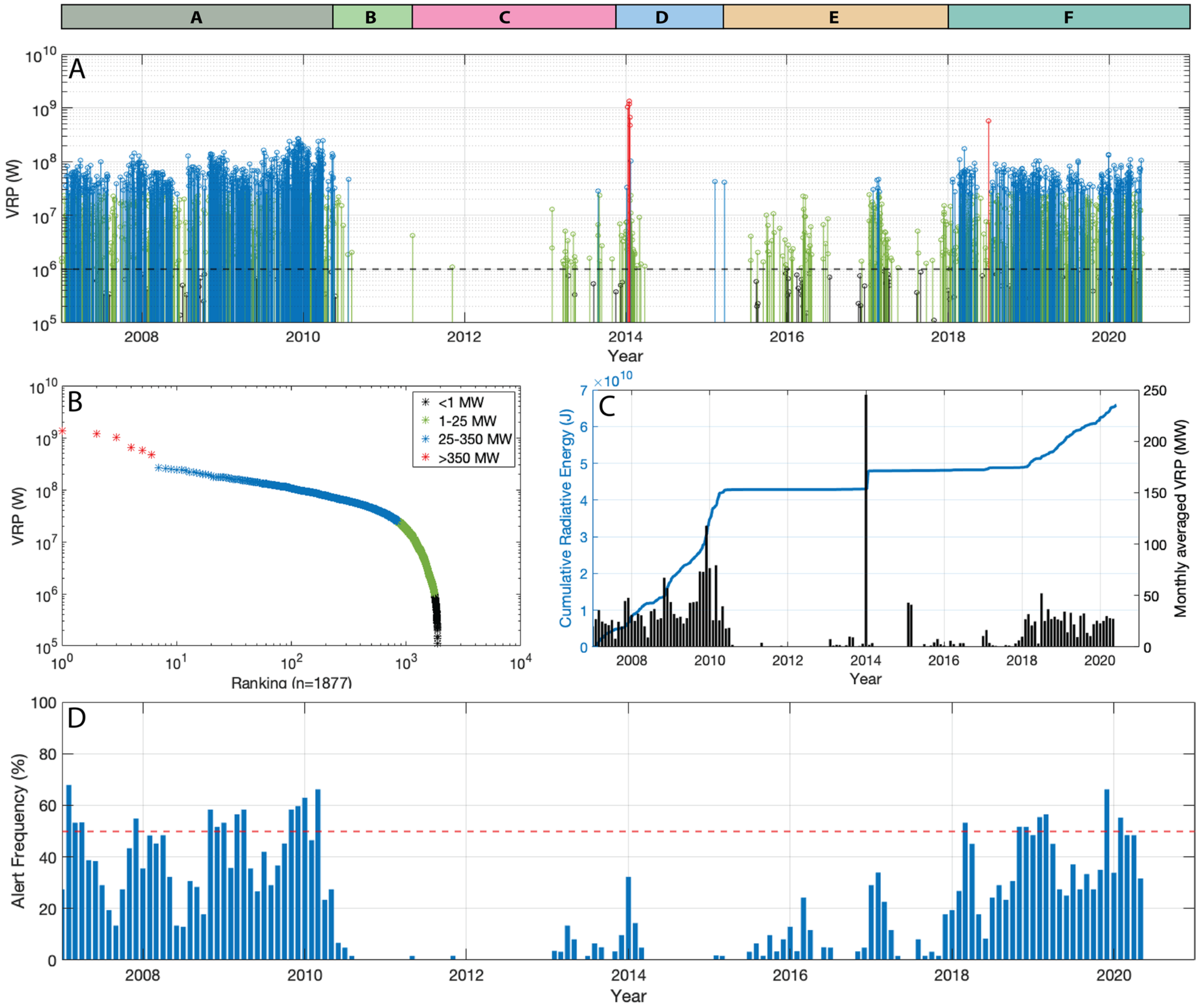

Fig. 6 Statistical analysis of MIROVA VRP data. The top banner shows the time periods identified from Fig. 4. **A** MIROVA-derived night-time log VRP at Pacaya, color-coded by the regimes identified from changes in slope in panel B. **B** Rank-order log–log plot of VRP, showing four distinct groupings in black, green, blue and red. **C** Cumulative radiative energy (blue) and monthly averaged VRP (black). D) Percentage of nights each month with a night-time MIROVA alert, with the red dashed line at 50%

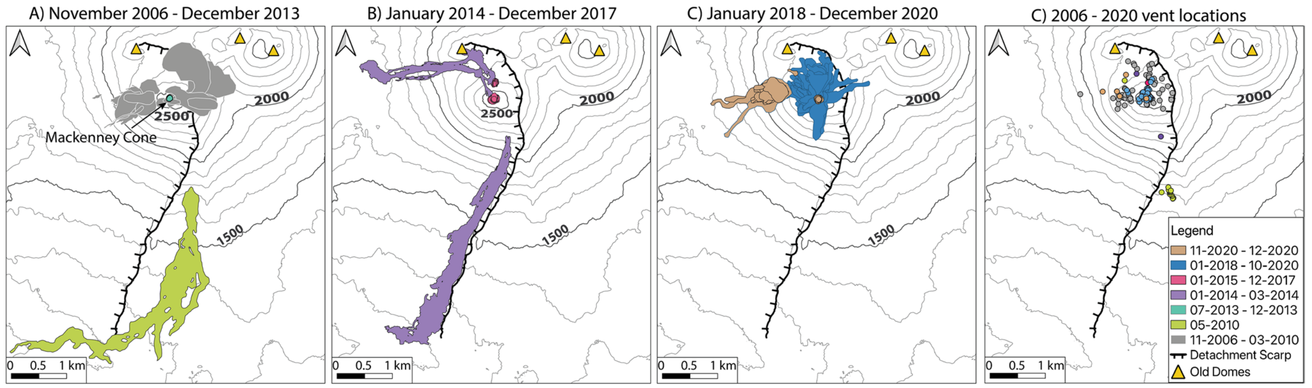

Fig. 7 Mapped lava flows from **A** 11–2006 to 12–2013; **B** 01–2014 to 12–2017; and **C** 01–2018 to 12–2020. D) Vent locations from 2006 to 2020, color-coded the same as the lava flows

Lava flow maps

Lava flows between 2006 and early 2010 are confined within 1 km of the summit (Fig. 7). The May 2010 flow originates from outside the collapse scarp on the south flank and extends for > 5 km. No flows were detected for the remainder of 2010, in 2011 or 2012. Crater incandescence was observed in late 2013, leading to the effusion of ~ 2.5 and ~ 4.8 km long west and south directed flows in January–March 2014, from vents along a north-northwest to south-southeast trend (Figs. 7, S1). Variable amounts of crater incandescence were recorded from 2015 to 2017. From 2018 to October 2020, lava flowed in variable directions from vents near the summit crater, with lengths < 1 km. November 2020 marked a transition to vent opening ~ 500 m west of the Mackenney cone, feeding flows up to ~ 1.4 km long, with continued summit crater incandescence.

Discussion

Flank motion modulated by magmatism

Compared to Gonzalez and Wauthier (2021), our new extended and denser time-series dataset reveals a pattern of repeated occurrence of faster flank creep initiating after major eruptions and transient flank motion events (2010, 2014), lasting on the order of a few months (periods B and D), followed by several years of slower flank creep with no major eruptions (periods C and E). We lack suitable InSAR or other ground-based geodetic datasets to assess whether flank deformation at Pacaya took place prior to 2007. Based on the available sparse ALOS-1 scenes, no significant displacement likely took place between mid-2007 and May 2010 (period A) (Figs. 4, S5, S6). Thus, assuming the surface displacements recorded thereafter are due to creep on the southwest flank of Pacaya, as proposed for between 2011 and 2014 by Gonzalez-Santana and Wauthier (2021), creep likely initiated during the vigorous May 2010 eruption. Previous InSAR studies identified ~ 4 m of flank motion during this eruption, making it one of the largest measured instability events that did not result in catastrophic collapse (Schaefer et al. 2015, 2017). Post-eruptive ALOS-1 interferograms showed subsequent flank-wide range increase, decreasing in extent and magnitude until early 2011 (Schaefer et al. 2016), in agreement with our time-series results (ALOS-1 c, Figs. 4, S7). Gonzalez-Santana and Wauthier (2021) attributed the ~ 2 cm/yr range increase in period C to slip on a southwest-dipping detachment fault, and the increase in rate in period D to forcing from dike intrusion during the January–March 2014 eruptions. Flank deformation during these 2014 eruptions was also of large enough magnitude to be captured by conventional differential InSAR, albeit less than recorded in 2010 (Schaefer et al. 2019; Wnuk & Wauthier 2017). Our extended dense time series (Fig. 4) confirms that flank creep continued beyond the January–March 2014 eruptions until 2018 (period E), when the range increase rate flattens out (period F). Furthermore, most of the range increase from 2015–2018 corresponds to subsidence of the southwest flank (Fig. 5). Unfortunately, the quality of the data near the summit is too poor to enable modeling of the sources of displacement beyond 2014. Instead, we assume that displacements between 2015 and 2018 are due to the same processes modeled for 2011–2014 by Gonzalez-Santana and Wauthier (2021).

All three thermal datasets showcase three periods of elevated thermal output, coincident with reported high activity periods, from 2007–2010 (A), during the 2014 eruptions (start of D), and from 2018 to 2020 (F) (Figs. 2 and 6). Comparing these datasets to the main transitions in flank creep behavior, we observe the following: negligible flank creep during elevated unrest (period A); onset and acceleration of flank creep, respectively, during the vigorous 2010 and 2014 eruptions (periods B and D); continued flank creep during relative volcanic quiescence (periods C and E); and disappearance of the clear creep trend during renewed elevated unrest (period F). Periods A and F coincide with increased reports of incandescence and elevated VRP and temperatures near the summit, suggesting that magma was being supplied to the surface through an open conduit.

Our study indicates that only the most vigorous eruptions appear to initiate (May 2010) or accelerate (January–March 2014) creep, whereas times of persistently restless/open-vent activity are not coincident with the initiation or acceleration of flank creep (A: 2007–2009, F: 2018–2020), implying that dike intrusion is a crucial driver of flank motion at Pacaya. When magma pathways are open, there is minimal forcing on the unstable flank. However, when more forceful intrusions associated to more vigorous and voluminous eruptions rupture the edifice beyond the open conduit, the flank slips. Both the 2010 and 2014 vents opened > 600 m away from the summit on the southern flank, producing the longest flows in the study period (> 4 km) (Figs. 7D, S1).

Renewed magmatic activity in 2017/2018 was likely not forceful enough to return the flank to an unstable state and opening of vents outside of the main crater area might be required to affect flank slip significantly. At volcanoes displaying flank creep, the slow deformation rate can allow elastic stresses to be relaxed, reducing the likelihood of development of normal faults and other discontinuities that can favor rapid flank failure (Van Wyk De Vries & Borgia 1996). Thus, flank creep identified in this study between 2010 and 2014 (periods B, C) and 2014–2018 (periods D, E) might have allowed the stresses in the edifice to relax, moving the flank away from failure.

Seasonal deformation and thermal signals

The annual cyclicity visible in LOS and vertical displacements (Figs. 4 and 5) can be attributed to seasonal variability in tropospheric water vapor. To compare the cyclicity in displacements with seasonal hydrologic variations, we compiled a rainfall time series from NASA/JAXA Tropical Rainfall Measurement Mission and Global Precipitation Measurement mission data (Farquharson & Amelung, 2020) (Fig. 8). This shows agreement in the phase of the annual cycles, with troughs in the LOS and vertical displacements corresponding to the timing of low rainfall in the boreal winter and peaks matching high rainfall in the boreal summer.

The substrate thickness required for the maximum annual precipitation of ~ 0.1 m to cause ~ 0.05 m true displacement of the ground is ~ 250 km, which is unrealistic (see Supplementary Material). Conversely, annual variations in tropospheric water vapor content over Pacaya can cause delay differences of ~ 10-cm amplitude, with peaks also in summer (Fig. S3).

Satellite geodetic studies of Central American volcanoes suffer from large contributions to interferometric phase from high variability and magnitude of tropospheric water vapor. In particular, the annual north–south migration of the Inter Tropical Convergence Zone leads to some of the largest water vapor variations in the world (Ebmeier et al. 2013a). The estimated resulting scatter in time-series over Pacaya is of up to ~ 5.3 cm (Ebmeier et al. 2013a), as observed here. We thus conclude that the source of the seasonal signals identified in this study are likely due to seasonal variations in tropospheric water vapor, as opposed to magma movements or ground dilation.

This tropospheric water vapor cyclicity is also reflected in MIROVA VRP and Alert Frequency (Fig. 6A, D). Despite near on-going lava effusion from 2007–2010 to 2018–2020, we observe peaks in VRP and alert frequencies in the dry boreal winter months, when fewer clouds obscure the thermal signals, and troughs in the wet boreal summer months, when cloud cover is probably greater.

No clear deformation signal associated with magma storage

A lack of clear InSAR-detected magmatic deformation has been recognized for volcanoes in the Central American Volcanic Arc, such as Pacaya (Ebmeier et al. 2013b). Based on our time-series results and interpretations we confirm that, aside from the aforementioned dike intrusions in 2010 and 2014, Pacaya does not clearly show magmatic deformation such as pre-eruptive inflation due to magma influx into reservoir(s). This is likely due to a combination of factors, such as (1) loss of coherence near the summit due to flank steepness and frequent changes in scattering properties from ashfall and intra-crater cone collapses, where deformation from shallow magma reservoir(s) would be expected; (2) the elevated detection threshold for deformation at Pacaya as a consequence of variability in tropospheric water vapor; (3) overprinting of smaller magnitude signals by the flank creep signal; or (4) specifics of magma composition and magma plumbing system geometry at Pacaya. The latter refers to a combination of controls on the geodetic expression of magma movements such as the flux, composition, storage geometry and depth, magma compressibility, and whether the conduit is open. Ground deformation from influx into vertically elongated reservoirs is of lower magnitude than that produced by spherical reservoirs (Ebmeier et al. 2013b). Additionally, in contrast to more evolved lavas, the basaltic lavas common at Pacaya rise directly from depth with minimal stalling in the crust. Their petrographic and chemical uniformity over time further imply continuous supply of magma to an open conduit, in agreement with rates of sulfur degassing in excess of what is expected from effusion rates (Ebmeier et al. 2013b; Eggers 1971; Matías Gomez et al. 2012).

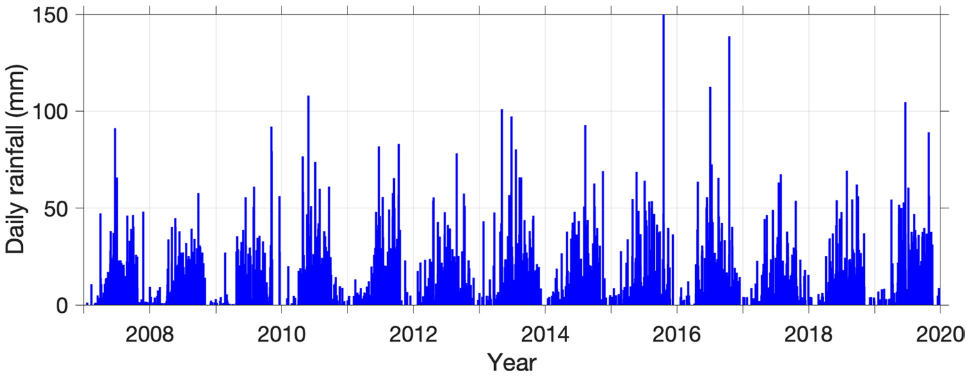

Fig. 8 Daily rainfall at Pacaya. The peak in October 2015 corresponds to landfall of Hurricane Patricia in Guatemala

Conceptual model for flank creep behavior at Pacaya Volcano

Our findings and interpretations suggest four different scenarios of volcanic activity and flank creep interactions at Pacaya (Fig. 9):

1. Open-conduit activity with negligible flank motion (2007–2009, 2018–2020),
2. Opening of new magma pathways during on-going eruptions with associated transient flank instability (2010),
3. Opening of new magma pathways after low volcanic activity with associated transient flank instability (2014),
4. New heightened activity with negligible flank instability (2017–2018).

Scenarios 1 and 2 apply to co-eruptive conditions, whereas 3 and 4 relate to inter-eruptive conditions. The subtle differences between these scenarios highlight the challenges in forecasting flank instability related hazards at Pacaya. For example, scenario 2 illustrates the secondary hazard from opening of a new vent during an apparently steady-state eruption. Identifying the transition from scenario 1 to scenario 2, as in May 2010, requires close monitoring of evolving eruptive activity. Similarly, whenever unrest is detected at a volcano, it is challenging to recognize whether this might result in scenario 3 or 4. The study of past vent locations and their association to each of the 4 scenarios can assist in forecasting the scenario new activity is most likely to cause.

Based on this study, it appears that since 2007 opening of new vents outside of the summit area, on the northwest and south-southeast flanks, irrespective of whether this marked the start or a transition in the eruption, has led to the initiation of transient flank instability at Pacaya. Thus, opening of new aligned vents outside the Mackenney cone forewarn an increased likelihood of renewed or accelerating flank creep.

Conclusions

Our study of the evolution of surface deformation on the southwest flank of Pacaya from 2007 to 2020 shows that flank creep initiated at the end of a heightened activity period, concurrently with a large explosive eruption in 2010, during which vents opened outside the ancestral collapse scarp. Furthermore, creep accelerated at the start of a new eruptive period in 2014 during which north-northwest to south-southeast oriented vents opened, also outside of the summit area. The rate of flank creep then decayed over a few years during low eruptive activity periods (2011–2013 and 2015–2018). We suggest that flank creep is triggered by forceful opening of new magma pathways, likely through diking, which can occur during an on-going eruption (2010) or at the start of a new eruption (2014). These events produce lava flows > 1 km long, from vents situated away from the main cone, and produce large thermal outputs. Resuming effusive activity near the main open conduit,

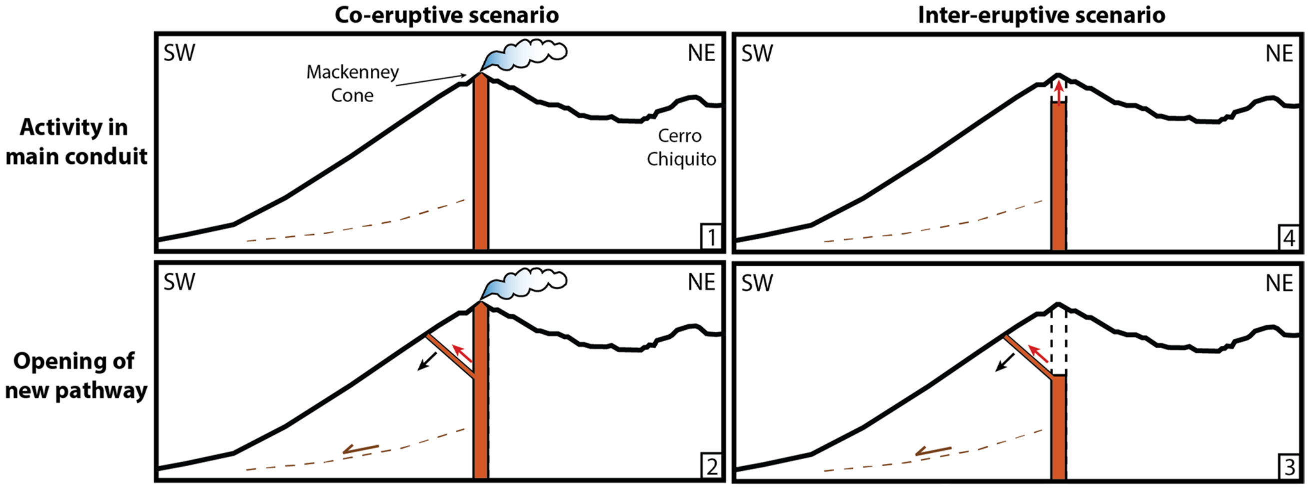

Fig. 9 Possible scenarios of volcanic activity and flank creep interactions at Pacaya. Conduit and detachment location and geometry are only approximate and not to scale. (1) open-conduit activity with negligible flank motion (2007–2009, 2018–2020). (2) Opening of new magma pathways during on-going eruptions with associated transient flank instability (2010). (3) Opening of new magma pathways after low volcanic activity with associated transient flank instability (2014). (4) New heightened activity with negligible flank instability (2017–2018)

on the other hand, does not appear to trigger flank creep (e.g., 2017, 2018). Our findings suggest that opening of new aligned vents outside the Mackenney cone summit area forewarns an increased likelihood of renewed or accelerating flank creep at Pacaya.

Supplementary Information The online version contains supplementary material available at https://doi.org/10.1007/s00445-022-01592-2.

Acknowledgements TanDEM-X digital elevation model data were provided through the German Aerospace Center (DLR Proposal ID 1552) and RADARSAT-2 SAR data were provided through CEOS, the Committee on Earth Observation Satellites Volcano Pilot and Demonstrator working groups (http://ceos.org/ourwork/workinggroups/disasters/volcanoes). COSMO-SkyMed data were obtained through both CEOS and ASI Cosmo-SkyMed Open Call for Science Proposal 731. We thank Diego Coppola for providing the MIROVA data, NASA and LPDAAC for access to ASTER data through the Earth Observing System Data and Information System, ESA for access to Sentinel-1 data and precise orbit files, the ASF Vertex DAAC for access to ALOS-1 data, and Planet Explorer for access to Sentinel-2 and Landsat-8 data. We thank Carla Chun for sharing the vent locations from 2006-2019 obtained during her undergraduate thesis at Universidad de San Carlos de Guatemala, in collaboration with INSIVUMEH. We thank Amilcar Roca, Gustavo Chigna, Roberto Merida, and Peter Argueta from INSIVUMEH, as well as Derek Elsworth, Charles Ammon, Damian Walwer, Kevin Reath, Gregory Waite, and Kirsten Stephens for useful discussions. We also thank Jamie Farquharson for sharing the rainfall time-series script. Computations were performed on The Pennsylvania State University's Institute for Computational and Data Sciences' Roar supercomputer.

Author contribution J. Gonzalez-Santana and C. Wauthier contributed to the study conception and design. Material preparation, data collection, and analysis were performed by J. Gonzalez-Santana under the supervision of C. Wauthier. Lava flow mapping was performed by M. Burns under the supervision of J. Gonzalez-Santana and C. Wauthier. The first draft of the manuscript was written by J. Gonzalez-Santana and all authors commented on previous versions of the manuscript. All authors read and approved the final manuscript.

Funding This work was supported by Future Investigators in NASA Earth and Space Science and Technology (FINESST) grant 80NSSC20K1632 and NASA Earth Surface and Interior grant 80NSSC20K0490, issued through the Science Mission Directorate's Earth Science Division.

Data availability Spreadsheets of compiled volcano activity reports are available as Supplementary Materials 2 and 3. A link to the lava flow and vent shapefiles repository is included in the Supplementary Text. Other data is available upon request from the authors.

Code availability InSAR processing was performed using the commercial software GAMMA. All derived products and additional code run on MATLAB are available upon request from the authors.

Declarations

Conflict of interest The authors declare no competing interests.

References

Bardintzeff JM, Deniel C (1992) Magmatic evolution of Pacaya and Cerro Chiquito volcanological complex Guatemala. Bull Volcanol 54(4):267–283. https://doi.org/10.1007/BF00301482

Berardino P, Fornaro G, Lanari R, Sansoti E (2002) A New algorithm for surface deformation monitoring based on small baseline differential SAR interferograms. IEEE Trans Geosci Remote Sens 40(11):2375–2383. https://doi.org/10.4088/JCP.12m08269

Chun C (2020) Actualización de mapas de amenaza por flujos de lava del volcán de Pacaya, San Vicente de Pacaya, utilizando modelos de procesos físicos y validación de campo. Undergraduate thesis, Universidad de San Carlos de Guatemala

Conway FM, Diehl JF, Matías O (1992) Paleomagnetic constraints on eruption patterns at the Pacaya composite volcano Guatemala. Bull Volcanol 55(1–2):25–32. https://doi.org/10.1007/BF00301117

Coppola D, Piscopo D, Laiolo M, Cigolini C, Delle Donne D, Ripepe M (2012) Radiative heat power at Stromboli volcano during 2000–2011: twelve years of MODIS observations. J Volcanol Geoth Res 215:48–60

Coppola D, Laiolo M, Cigolini C, Delle Donne D, Ripepe M (2016) Enhanced volcanic hot-spot detection using MODIS IR data: results from the MIROVA system. Geo Soc London Spec Publ 426(1):181–205

Costantini M (1998) A Novel phase unwrapping method based on network programming. IEEE Trans Geosci Remote Sens 36(3):813–821. https://doi.org/10.1109/36.673674

Costantini M, Rosen PA (1999) A generalized phase unwrapping approach for sparse data. IEEE 1999 Int Geosci Remote Sensi Symp IGARSS'99 (Cat. No. 99CH36293 1:267–269. https://doi.org/10.1109/IGARSS.1999.773467

Dufresne A, Siebert L, Bernard B (2020) Distribution and geometric parameters of volcanic debris avalanche deposits. In Volcanic Debris Avalanches (pp. 75–90). Springer

Ebmeier SK, Biggs J, Mather TA, Amelung F (2013a) Applicability of InSAR to tropical volcanoes: insights from central america. Geol Soc Spec Pub 380(1):15–37. https://doi.org/10.1144/SP380.2

Ebmeier SK, Biggs J, Mather TA, Amelung F (2013b) On the lack of InSAR observations of magmatic deformation at Central American volcanoes. J Geophys Res Solid Earth 118(5):2571–2585. https://doi.org/10.1002/jgrb.50195

Eggers A (1971) The geology and petrology of the Amatitlán quadrangle, Guatemala. Dartmouth College

Elsworth D, Voight B (1995) Dike intrusion as a trigger for large earthquakes and the failure of volcano flanks. J Geophys Res Solid Earth 100(B4):6005–6024

Farquharson JI, Amelung F (2020) Extreme rainfall triggered the 2018 rift eruption at K{\=\i}lauea Volcano. Nature 580(7804):491–495

Gillespie A, Rokugawa S, Matsunaga T, Steven Cothern J, Hook S, Kahle AB (1998) A temperature and emissivity separation algorithm for advanced spaceborne thermal emission and reflection radiometer (ASTER) images. IEEE Trans Geosci Remote Sens 36(4):1113–1126. https://doi.org/10.1109/36.700995

Global Volcanism Program (2013) Pacaya (342110) in {Volcanoes of the World, v. 4.7.5 Venzke, E (ed.). Smithsonian Institution}

Goldstein RM, Werner CL (1998) Radar interferogram filtering for geophysical applications. Geophys Res Lett 25(21):4035–4038. https://doi.org/10.1029/1998GL900033

Gonzalez-Santana J, Wauthier C (2021) Unraveling long-term volcano flank instability at Pacaya Volcano, Guatemala, using satellite geodesy. J Volcanol Geoth Res 410:107147

Kitamura S, Matias O (1995) Tephra stratigraphic approach to the eruptive history of Pacaya Volcano, Guatemala. In Scie Rep Tohoku Univ 45(1):1–42

Lundgren P, Usai S, Sansosti E, Lanari R, Tesauro M, Fornaro G, Berardino P (2001) Modeling surface deformation observed with synthetic aperture radar interferometry at Campi Flegrei caldera. J Geophys Res Solid Earth 106(B9):19355–19366. https://doi.org/10.1029/2001jb000194

Matías Gomez RO, Rose WI, Palma JL, Escobar-Wolf R (2012) Notes on a Map of the 1961 – 2010 Eruptions of Volcán de Pacaya, Guatemala. The Geological Society of America Digital Map and Chart Series 10. https://doi.org/10.1130/2012.DMCH010

McGuire WJ (2003) Volcano instability and lateral collapse. Revista I:33–45

Naismith AK, Watson IM, Escobar-Wolf R, Chigna G, Thomas H, Coppola D, Chun C (2019) Eruption frequency patterns through time for the current (1999–2018) activity cycle at Volcán de Fuego derived from remote sensing data: Evidence for an accelerating cycle of explosive paroxysms and potential implications of eruptive activity. J Volcanol Geoth Res 371:206–219

National Oceanic and Atmospheric Administration (NOAA) (2021) Current Washington VAAC Volcano Ash Advisory Archive. https://www.ssd.noaa.gov/VAAC/archive.html. Accessed 20 Feb 2021

Poland MP, Peltier A, Bonforte A, Puglisi G (2017) The spectrum of persistent volcanic flank instability: a review and proposed framework based on Kīlauea, Piton de la Fournaise, and Etna. J Volcanol Geoth Res 339:63–80. https://doi.org/10.1016/j.jvolgeores.2017.05.004

Reath K, Pritchard ME, Moruzzi S, Alcott A, Coppola D, Pieri D (2019a) The AVTOD (ASTER Volcanic Thermal Output Database) Latin America archive. J Volcanol Geoth Res 376:62–74

Reath K, Pritchard M, Poland M, Delgado F, Carn S, Coppola D, Andrews B, Ebmeier SK, Rumpf E, Henderson S et al (2019b) Thermal, deformation, and degassing remote sensing time series (CE 2000–2017) at the 47 most active volcanoes in Latin America: Implications for volcanic systems. J. Geophys. Res. Solid Earth 124(1):195–218

Rose WI, Palma JL, Wolf RE, Matías Gomez RO (2013) A 50 yr eruption of a basaltic composite cone: Pacaya, Guatemala. Geol Soc Am Spec Pap 498:1–21. https://doi.org/10.1130/2013.2498(01)

Roverato M, Di Traglia F, Procter J, Paguican E, Dufresne A (2020) Factors contributing to volcano lateral collapse. In Volcanic Debris Avalanches (pp. 91–119). Springer

Samsonov S, d'Oreye N (2012) Multidimensional time-series analysis of ground deformation from multiple InSAR data sets applied to Virunga Volcanic Province. Geophys J Int 191(3):1095–1108

Samsonov SV (2019) User manual, source code, and test set for MSBASv3 (Multidimensional Small Baseline Subset version 3) for one-and two-dimensional deformation analysis. Geomatics Canadaa

Samsonov SV, d'Oreye N (2017) Multidimensional small baseline subset (MSBAS) for two-dimensional deformation analysis: Case study Mexico City. Can J Remote Sens 43(4):318–329

Schaefer L, Lu Z, Oommen T (2015) Dramatic volcanic instability revealed by InSAR. Geology 43(8):743–746. https://doi.org/10.1130/G36678.1

Schaefer LN, Lu Z, Oommen T (2016) Post-eruption deformation processes measured using ALOS-1 and UAVSAR InSAR at Pacaya Volcano Guatemala. Remote Sensing 8(1):1–15. https://doi.org/10.3390/rs8010073

Schaefer LN, Wang T, Escobar-Wolf R, Oommen T, Lu Z, Kim J, Lundgren PR, Waite GP (2017) Three-dimensional displacements of a large volcano flank movement during the May 2010 eruptions at Pacaya Volcano Guatemala. Geophys Res Lett 44(1):135–142. https://doi.org/10.1002/2016GL071402

Schaefer LN, Di Traglia F, Chaussard E, Lu Z, Nolesini T, Casagli N (2019) Monitoring volcano slope instability with Synthetic Aperture Radar: a review and new data from Pacaya (Guatemala) and Stromboli (Italy) volcanoes. Earth Sci Rev 192:236–257. https://doi.org/10.1016/j.earscirev.2019.03.009

Siebert L, Glicken H, Ui T (1987) Volcanic hazards from Bezymianny- and Bandai-type eruptions. Bull Volcanol 49:435–459

Siebert L, Alvarado GE, Valance JW, vanWyk de Vries, B. (2006) Large-volume volcanic edifice failures in Central America and associated hazards. Volcanic Haz Central Am Geologic Soc Am Spec Pap 412(01):1–26. https://doi.org/10.1130/2006.2412(01)

Vallance JW, Siebert L, Rose WI, Girón JR, Banks NG (1995) Edifice collapse and related hazards in Guatemala. J Volcanol Geoth Res 66(1–4):337–355. https://doi.org/10.1016/0377-0273(94)00076-S

Van Wyk De Vries B, Borgia A (1996) The role of basement in volcano deformation. Geol Soc Spec Publ. 110(1), 95–110

Wardman J, Sword-Daniels V, Stewart C, Wilson TM (2012) Impact assessment of theMay 2010 eruption of Pacaya volcano, Guatemala: GNS Science Open-File Report 2012/09

Werner C, Wegmuller U, Strozzi T, Wiesmann A (2001) GAMMA SAR and Interferometric Processing Software. Proceedings of the ERS-Envisat Symposium, Gothenburg

Wnuk K, Wauthier C (2017) Surface deformation induced by magmatic processes at Pacaya Volcano, Guatemala revealed by InSAR. J Volcanol Geoth Res 344:197–211. https://doi.org/10.1016/j.jvolgeores.2017.06.024

Wright R (2016) MODVOLC: 14 years of autonomous observations of effusive volcanism from space. Geol Soc Spec Pub 426(1):23–53. https://doi.org/10.1144/SP426.12

Wright R, Flynn LP, Garbeil H, Harris AJL, Pilger E (2004) MODVOLC: near-real-time thermal monitoring of global volcanism. J Volcanol Geoth Res 135(1–2):29–49

Zernack AV, Procter JN (2021) Cyclic growth and destruction of volcanoes. In Volcanic Debris Avalanches (pp. 311–355). Springer